DE GRUYTER DOI 10.1515/zpch-2014-0438 — Z. Phys. Chem. 2014; 228(4–5): 587–607

Christin Büchner, Philomena Schlexer, Leonid Lichtenstein, Stefanie Stuckenholz, Markus Heyde*, and Hans-Joachim Freund

Topological Investigation of Two-Dimensional Amorphous Materials

Abstract: Real space image data of two-dimensional amorphous networks have become available in high resolution. We review a number of systems regarding ring size distribution, pair correlation function and characteristic structural clusters. We present similarities and differences that can help identify general descriptors for amorphousness.

Keywords: Amorphous, Vitreous, Glass, Non-Crystalline, Crystalline, Network, Two-Dimensional.

***Corresponding Author: Markus Heyde,** Fritz-Haber-Institut der Max-Planck-Gesellschaft, Faradayweg 4-6, 14195 Berlin, Germany, e-mail: heyde@fhi-berlin.mpg.de
Christin Büchner, Philomena Schlexer, Leonid Lichtenstein, Stefanie Stuckenholz, Hans-Joachim Freund: Fritz-Haber-Institut der Max-Planck-Gesellschaft, Faradayweg 4-6, 14195 Berlin, Germany

Dedicated to: Professor Klaus Rademann on the occasion of his 60th birthday

1 Introduction

Structure elucidation is a key factor in understanding properties and behavior of any material and of course for developing novel materials. With today's analytical tools, researchers are able to identify the structure of a vast number of crystalline materials. For non-crystalline materials, however, structural data and hence a comprehensive model to describe and compare systems is harder to come by. The definitions of crystallinity and amorphousness reflect the dilemma that structural research faces. Crystals are highly periodic, whereas amorphous materials possess short-range order, but lack long-range order and periodicity. While the crystal can easily be described with some unit cell coordinates and information on lattice symmetry, the non-periodic structure evades such precise classification. A vast number of structure models have been proposed, the most famous being the random network theory by W. H. Zachariasen [1]. His ideas were

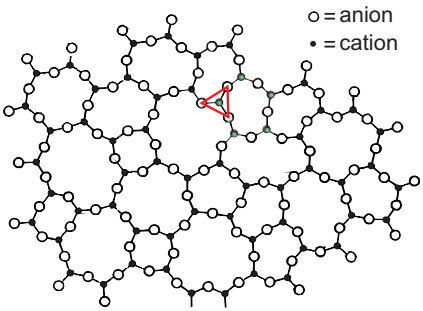

Figure 1: Random network model by W. H. Zachariasen [1]. Based on diffraction data of oxide materials, a network of identical building blocks with varying bridging angles was proposed for amorphous solids. In this two-dimensional representation, one building unit is marked with a red triangle, corresponding to a tetrahedron in three-dimensional materials. Green circles mark a few of the cation positions (Si in the case of silica glass). The cation positions marked here make up a five-membered ring (pores are the three-dimensional analogon).

entirely based on his knowledge of macroscopic properties of glasses and X-ray diffraction data. According to his random network theory, glasses consist of small building units that have similar short-range order as a crystalline compound of the same chemical formula. These building units are linked by the same forces as in crystals. The crucial ingredient for amorphous materials are random bond angles between building units which form an extended network with essentially an infinitely large unit cell [1]. Figure 1 shows Zachariasen's concept for a two-dimensional network of a species A_2O_3. The small building unit is a triangle with a cation A in the center and an anion O at each corner (marked with a red triangle). These building blocks exhibit uniform symmetry everywhere throughout the network, but they are linked at various angles over bridging O atoms. Hence, they form closed chains of different sizes. Depending on the number s of the involved cations, we call them s-membered rings or s-membered polygons. In Figure 1, five cations are marked with green circles. They comprise a five-membered ring. In his publication, Zachariasen chose this two-dimensional visualization simply for clarity, not anticipating that the two-dimensional approach would be the final step in resolving the atomic structure of glass. Even though direct proof for Zachariasen's theory remained absent for 80 years, the random network theory was universally accepted and became the standard textbook model.

A new chapter in the investigation of amorphous materials was opened with the introduction of scanning probe techniques, radically lowering the resolution limit. The inventors of scanning tunneling microscopy (STM) and electron microscopy were awarded with the Nobel Prize for their achievements in 1986, however, true atomic resolution on an amorphous surface was only achieved in

2012 [2, 3]. Amorphous bulk materials, also being amorphous at their surfaces, are simply too uneven in the direction perpendicular to the surface (z-direction), to allow high resolution images with the available techniques. Many attempts to achieve atomic resolution of cleaved bulk oxide glasses or metallic glasses have been made in the past decades [4–10]. Bürgler *et al.* [6] described the problem that higher-lying atoms topographically block or shield the lower-lying atoms as the "hiding effect".

The problem of very rough amorphous surfaces was circumvented by borrowing a thin film approach from model catalysis [11]. A well-defined ultrathin film of amorphous silicon dioxide finally allowed microscopy based structure revelation of an unordered SiO_2 bilayer film [2]. Ultimately, it was found to be a continuous random network, exactly as described by Zachariasen in 1932. Another group was able to verify these findings for a silica bilayer on graphene, using transmission electron microscopy [3].

With these advancements in structural research, the natural question to ask would be: is it possible to find a means of classification for amorphous solids? Crystalline materials allow unequivocal description with a few parameters. What features can be used as defining properties in the comparison of unordered substances? A milestone publication dealing with this concern was presented in 1984 by Weaire and Rivier [12]. Here, a huge number of non-ordered natural and theoretical systems were presented and many different concepts of classification and comparison were described. Due to the extreme inhomogeneity of the presented networks, a universal description fitting all systems could not be proclaimed.

A. C. Wright *et al.* [13] proposed a very direct way of defining a random network quantitatively on the basis of diffraction data. They divided the network into different ranges from I to IV. The regular building blocks of glasses are defined as range I, or the structural unit. Adjacent connected units make up range II. Network topology is the subject matter of range III and range IV describes larger structural fluctuations. Characteristic parameters are then assigned to quantify each range of network order. Coordination numbers, distributions of bond lengths or angles and ring size distribution can be evaluated, for example. For covalent amorphous networks, scanning probe techniques have enabled the investigation of these parameters, since high resolution images provide sufficient data.

In this paper, we will compare a variety of systems, ordered and unordered, and on different length scales. In order to analyze the different networks in a coherent fashion, the concept of a connection point was defined. It originates from the observation that the Si positions in the silica network, connected to their nearest neighbors, span a plane tiled with differently sized polygons. These polygons or rings can be analyzed according to their abundance and occurring combinations in order to gain insight into the factors influencing network formation. In

analogy to the silica network, a connection point is defined as a triple coordinated center of a structural unit. The connection point does not necessarily have to coincide with an atomic position. The main criterion for including a system in the study, is the coordination $z = 3$ for each connection point. A second condition is a narrow distribution of distances between connection points (nearest neighbor or NN distances). Strong similarities of all systems regarding A. C. Wright's range I allow us to focus on features of the range II and III. We will especially evaluate ring size distributions, pair distance distributions and characteristic topological clusters.

2 Two-dimensional networks

Our approach is to compare a number of networks, in order to find similarities in their medium range order. To this end, we selected eight two-dimensional network systems, which all possess threefold coordination in their building blocks.

The first system is a two-dimensional crystalline SiO_2 sheet on a Ru(0001) substrate. An STM image of this thin film is shown in Figure 2, revealing the Si positions. The preparation of such a silica layer was described by Löffler *et al.* [14]. In the ordered film, SiO_4-tetrahedra are connected over oxygen bridges with uniform bonding angles and form a regular honeycomb lattice on the substrate crystal. Half of the topography image is superimposed with small green circles to mark the positions of silicon atoms, which represent the connection points in this system. Only six-membered rings are formed (indicated by large green circles). The ring size statistic on the right side shows the number of rings with sizes s that occur in the evaluated image.

The 7×7 reconstruction of Si(111) (shown in the bottom part of Figure 2) is crystalline as well, but not quite as simple. It forms upon annealing of a cleaved Si(111) surface and is stable up to temperatures of $\sim 1000\,^{\circ}C$ [15]. STM images reveal only the top layers of the atoms involved in this reconstruction [16]. The topography image is derived from the established **D**imer **A**datom **S**tacking fault (DAS) model for this surface, [17] green circles mark Si positions. A black rhombus marks the unit cell of the 7×7 reconstruction. The silicon atoms form rings of different sizes, marked in colored larger circles. The ring size histogram shows that not all conceivable ring sizes occur. The number of five-, six- and eight-membered rings for one unit cell of the lattice is shown. Additionally, one 12-membered ring per unit cell is observed.

Figure 3 presents an amorphous SiO_2 film in the top part and a triangle raft model for glasses proposed by Shackelford and Brown [19] in the bottom part.

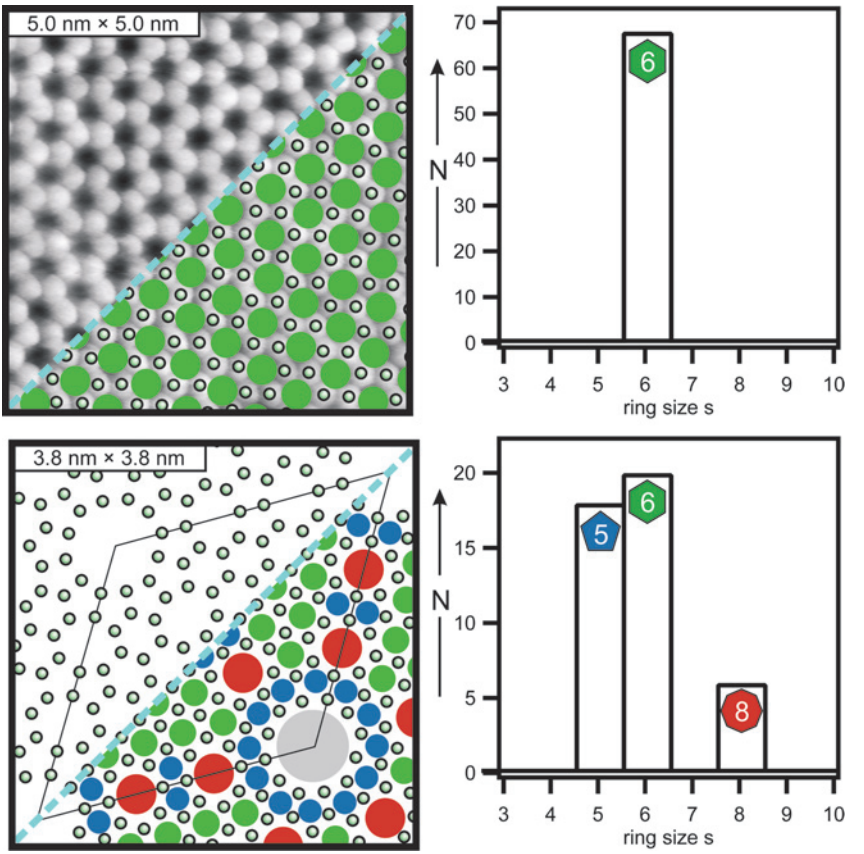

Figure 2: Top: STM image of a crystalline SiO_2 sheet [taken from [18]] (image: $V_S = 3$ V, $I_T = 100$ pA). The contrast reveals the Si positions of the SiO_2 film, which are partly marked with small green circles. Six-membered rings (marked with large green circles on part of the image) are the only ring size in this highly ordered system, as is shown in the corresponding ring size histogram on the right. Bottom: Model of a Si(111) surface in the 7×7 reconstruction [17]. A rhombus shape indicates the unit cell. Si positions are marked with small green circles, different ring sizes are marked in different colors on part of the model. The ring size histogram on the right shows the occurence of five-, six- and eight-membered rings in this complex crystalline surface. Only the rings within one unit cell of the 7×7 reconstruction were counted for the histogram. The unit cell also contains one 12-membered ring.

The vitreous silica bilayer was prepared according to the procedure described in [2]. nc-AFM images were taken with a custom-built UHV microscopy setup using a quartz tuning fork sensor at low temperatures. The image presented in this work was acquired in constant-height mode. Oxygen atoms are visible in this nc-AFM contrast (for a discussion of element-sensitive imaging modes see [18]). Silicon po-

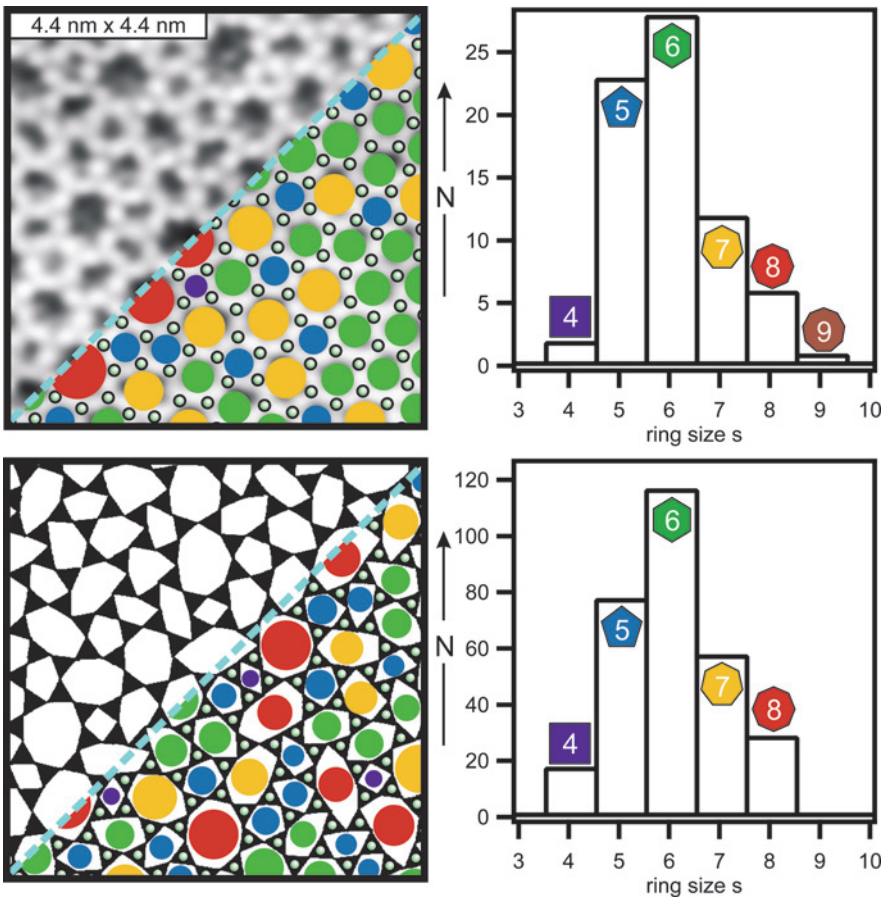

Figure 3: Top: nc-AFM image reveals the atomic structure of an amorphous SiO_2 bilayer, the Si positions are marked with small green circles (image: $V_S = 100\,\mathrm{mV}$, constant height mode). Different sized rings are marked with respective colors and partially superimposed on the STM image. The complete ring size histogram of this dataset is presented on the right side. Four- to nine-membered rings occur, six-membered rings exhibit the highest occurrence. Bottom: The image shows a triangle raft suggested by J. Shackelford as a model for amorphous SiO_2 networks [19]. Connection points in the center of the traingles are marked with small green circles. The differently sized polygons are indicated with corresponding colors on part of the topography image. The algorithm for creating the triangle raft limits possible ring sizes from four to eight. On the right hand side, the ring size histogram shows ring sizes from four to eight, with six-membered rings as the most abundant. The ring size histograms of both systems show good agreement concerning the relative frequency of ring sizes. Five-membered rings are occurring more often than seven-membered rings in both systems, and eight-membered rings are more common than four-membered rings.

sitions are determined in the center of each oxygen triangle (marked with small green circles). Pores of different sizes can be observed and are indicated by colored circles on part of the topography image. The ring size histogram on the right side shows that six-membered rings are the most abundant species. In contrast to crystalline SiO_2, where six-membered rings are the only species, five-membered rings are also occurring very often, followed by seven- and eight-membered rings. The bottom part of Figure 3 shows the topography image of a triangle raft on the left side [19]. This model system was created as a tool to visualize the random network structures proposed by Zachariasen [1]. An algorithm was proposed to randomly arrange equilateral triangles, corresponding to the building blocks in Zachariasen's two-dimensional concept of glass. In the algorithm, only ring sizes from four to eight were allowed. A part of a resulting triangle raft is shown in the bottom of Figure 3, with small green circles indicating the threefold coordinated connection points. Differently sized polygons are marked with colored circles. The ring size statistic shows a distribution similar to that of amorphous silica. Six-membered rings are most abundant, followed by five-, seven- and eight-membered rings. In this distribution, Shackelford found a lognormal behavior and postulated that a lognormal ring size distribution was a general feature of amorphous networks.

The top part of Figure 4 shows a theoretical model for amorphous graphene. This model was published by Li and Drabold [20]. Other groups have been working with amorphous carbon models as well [21] and experimentalists are trying to create amorphous graphene by e-beam irradiation, [22–24] or reduction of graphene oxide [25]. These methods typically yield isolated defects and small amorphous patches embedded in mostly crystalline graphene sheets. The model of an amorphous graphene sheet presented by Li *et al.* [20] was large enough to allow statistical evaluation. Carbon positions are marked with small green circles and the different sized rings with larger colored circles. The ring size histogram shows a high abundance of six-membered rings and almost as many five-membered rings. No four-membered rings are observed in the model, even though four- to nine-membered carbon rings were observed in e-beam irradiated graphene sheets by Kotakoski *et al.* [22]. In the graphene sheet model presented by Li *et al.*, [20] two 12-membered rings were also observed but are treated as negligible since they amount to less than 1% of the total number of rings.

The bottom part of Figure 4 depicts an intermediate Cu_2O network, presented by F. Yang *et al.* [26]. It is prepared *via* partial oxidation of a clean Cu(111) surface at 550 K. Details of the preparation and STM imaging are described in [26]. In the two-dimensional network, Cu_3O^+ triangles form the structural building block [27]. Connection points are oxygen atoms at the triangle centers, on part of the topography image they are indicated with small green circles. This metastable structure

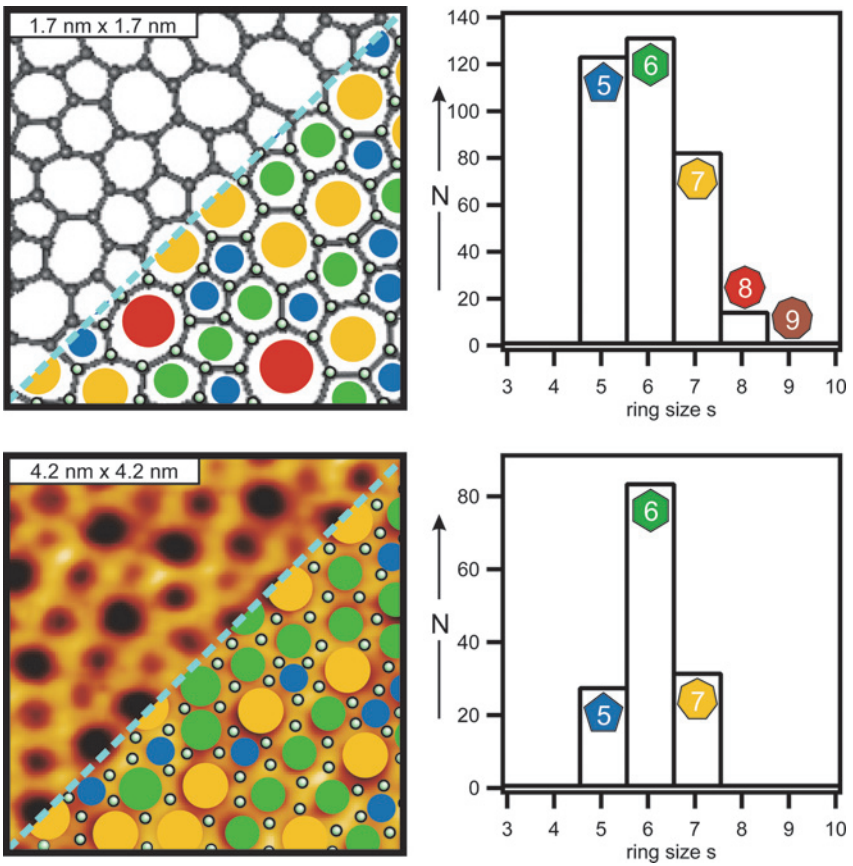

Figure 4: Top: computational model for a sheet of amorphous graphene [20]. On part of the image, C positions are indicated with small green circles and different ring sizes are shown with colored circles. In addition to the five- to nine-membered rings shown in the ring size histogram on the right side, the published graphene sheet possessed two 12-membered rings. Bottom: an STM image of a defect-rich $Cu_2O(111)$ surface is shown [26] (image: $V_S = -1.0\,\mathrm{V}$, $I_T = 100\,\mathrm{pA}$). It is partly superimposed with small green spheres at the O positions and colored circles indicating polygon size. In the Cu_2O, only five-, six- and seven-membered rings are observed. Both systems lack ring sizes smaller than five connection points.

evolves into crystalline Cu_2O upon longer oxidation treatment. The intermediary surface forms pores of five, six or seven connection points, indicated with colored circles in the STM image in Figure 4. The ring size histogram on the right side reveals that in this case, there are slightly more seven- than five-membered rings. The six-membered ring, which constitutes the structure element of the fully oxidized, crystalline film, is again the most frequent species.

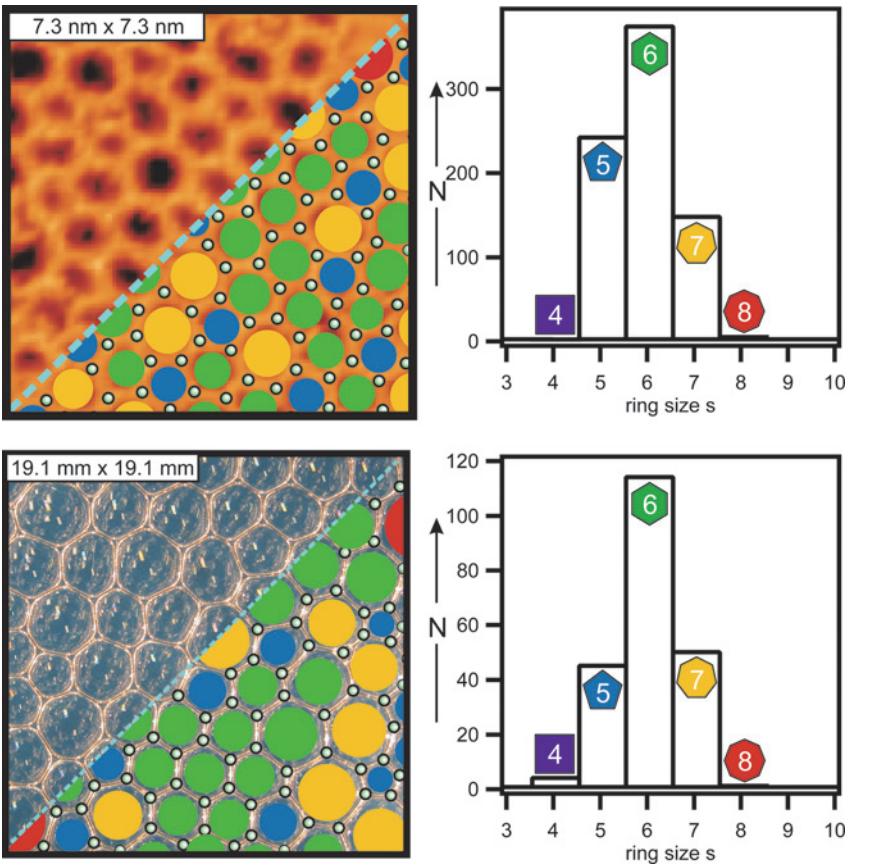

Figure 5: Top: STM image of an amorphous film of polymerized TBPB-Molecules on a Au(111) substrate [28]. The individual molecules possess a trigonal geometry. Annealing leads to an extended network of covalently linked TBPB-units. The former molecule centers constitute the connection points of the resulting amorphous network, marked with small green circles. Larger circles in different colors show the different polygons. Rings from four to eight connection points are observed, as shown in the histogram on the right side. Bottom: Photo of a macroscopic bubble raft. Soap bubbles form a space-filling arrangement that exhibits different sized polygons (shown with colored circles) and lacks long-range order. The histogram on the right side shows that ring sizes from four to eight are observed.

The top part of Figure 5 presents a network of polymerized 1,3,5-tris(4-bromophenyl)benzene (TBPB) molecules on a Au(111) substrate. This structure was prepared by Blunt *et al.* [28] *via* deposition of ~ 0.25 ML TBPB molecules on a hot Au surface and subsequent annealing. The idea to prepare a porous two-dimensional network structure by polymerizing a layer of self-assembled organic

molecules, was first realized by Grill *et al.* [29]. Using a monomer with a trigonal shape, Blunt *et al.* were able to produce an irregular network with different pore sizes. In the center of each triangular unit lies the connection point, marked by a small green circle. The regular building blocks are connected at random angles, polygons of different sizes are indicated with different colors on the STM image. The ring size statistic shows a large number of six-membered rings. However, in the case of this molecule network, no completely hexagonal phase has been presented yet. Instead, coverages of around one monolayer rather lead to densely packed arrangements of TBPB dimers [28, 30].

The photograph at the bottom of Figure 5 shows a bubble raft, prepared in our department. Bubble rafts can be employed to study phenomena like crystalline order, defects and also amorphousness. The concept of using bubble rafts as macroscopic model systems for crystalline packing and defects was first introduced by Bragg *et al.* in 1947 [31]. The bubble raft was prepared in a solution of surfactant and glycerin, consistent with the recipe described by Bragg [31]. Soap bubbles are produced by pumping a stream of air through a syringe needle. Low air pressure produces uniformly sized bubbles that arrange in crystalline-like order. Using a higher air pressure we produced non-uniform bubbles. A connection point is defined as the center of a triplet of bubbles that are tangent to one another without any additional bubbles in between. Since the network formation in this system is not defined through chemical bond lengths, a strong variation of connection point NN distances can be observed. Hence, two bubbles, which both are enclosed by six connection points, can have very different radii. Constructing a bubble raft without size variation restraints produces rafts exhibiting apollonian packing where the void between three bubbles may be occupied by a significantly smaller bubble. For the presented comparative study we selected a dataset with a relative variation of bubble radii in the same range as the relative variation of silica pore radii to avoid such fractal-like structures. The connection points are partly indicated on the photo with small green circles, larger colored circles mark different bubble sizes. The ring size histogram shows that ring sizes from four to eight connection points were observed.

3 Discussion

In the previous section, different two-dimensional networks were introduced. They all have a characteristic ring size distribution. This characteristic can be used to compare different amorphous systems. For all of the investigated systems, six-membered rings were the most abundant species. From the ring size

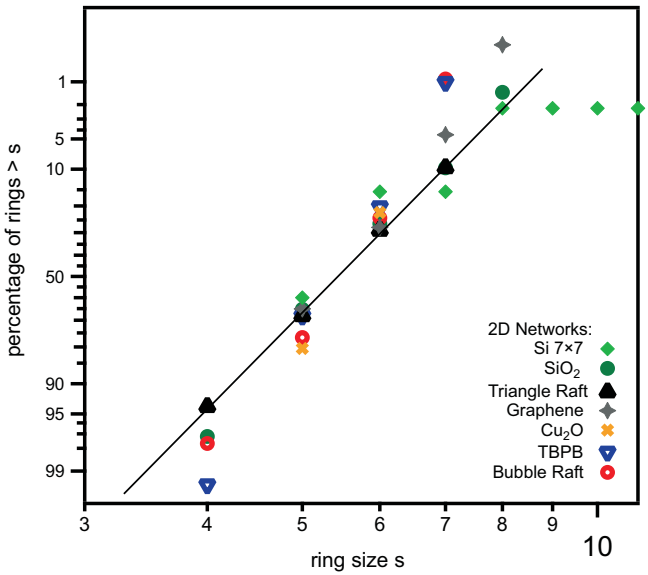

Figure 6: Lognormal plot of ring size distributions. Plotted in a lognormal probability plot, the ring size distributions of most systems exhibit linear behavior. A straight line is indicating the trend of the triangle raft ring size distribution. Amorphous SiO_2, graphene and the TBPB network all show a linear behavior, with respectively increasing slope. The data of the bubble raft clearly deviate from a linear behavior and the Si 7×7 surface shows non-linear behavior as well.

statistics presented in the preceding passage, it is clear that the distributions are skewed with respect to a symmetrical Gaussian distribution. Therefore, we treat them as lognormal distributions, where not the ring size s, but $\log(s)$ is normally distributed [32]. In an effort to test Shackelford's hypothesis that all amorphous systems exhibit a lognormal distribution, we plotted the ring size distributions of the investigated systems in a lognormal probability plot (Figure 6). In this depiction, the logarithmic x-axis is the ring size and the y-axis shows the probability of finding a ring size larger than s. Lognormally distributed data are arranged in a straight line in this plot. A straight line is drawn through the points of Shackelford's triangle raft network, to act as a guide to the eye. The crystalline SiO_2 film is omitted, since it only has six-membered rings. Also, the Cu_2O network only gives two relevant data points (different from 100% or 0%) for this depiction, which are merely plotted for completeness. The values for amorphous silica follow the behavior of the Shackelford data very closely. In the case of the amorphous graphene sheet and the TBPB molecule network, one can also assume a linear behavior with varying slopes. For the values of the bubble raft, however, a non-linear behavior

would be better suited to fit the data presented. The deviation from the predicted lognormal distribution in the case of the bubble raft, might be explained with the lack of limitations for ring forming processes. While in the other networks, chemical bond length and bond angle variations determine the ring structures that are able to form, such precise conditions are absent for the bubble rafts. As a result, polygons with the same number of edges can have very different areas. This circumstance influences the mechanisms of packing and space filling and, consequently, the ring size distribution. For the Si 7×7 reconstruction, the ring size distribution for one unit cell is plotted. From the histogram in Figure 2 we saw that only specific ring sizes occur in this crystalline structure and their number per unit cell is predefined. In the lognormal plot, the Si 7×7 values deviate strongly from linear behavior, which is consistent with the initial hypothesis, that the lognormal behavior is characteristic for amorphous systems.

We can conclude from the comparative lognormal ring size plot, that Shackelford's hypothesis holds for random networks in a certain range. If the network formation is not confined by fixed spacing parameters such as a chemically defined bond length, the resulting network is "too random" and ring size statistics may deviate from the lognormal distribution. The Si 7×7 reconstruction exhibits rings of different size, but they are not randomly distributed and do not fit a lognormal distribution, either.

Probability theory provides us with two descriptors that each capture a property of the ring size distribution in one number. These are the second and third central moment of the ring size probability distribution, μ_2 and μ_3. They are determined using the general equation

$$\mu_k = \sum_n (n-6)^k p(n), \tag{1}$$

Where n is the ring size, $p(n)$ the probability distribution of ring sizes and k is 2 or 3 for μ_2 or μ_3, respectively. The value six is the so-called expectation value of the ring size, which can be directly derived from Euler's Formula (for detailed information, see the supplement). Weaire *et al.* made use of this concept [12] and Wilson *et al.* employed the second central moment (using a different notation) to describe several amorphous SiO_2 model networks [33]. The second central moment μ_2 describes the variance of a distribution around the mean value. The results for all networks investigated in this study are presented in Table 1. Due to the $(n-6)^2$ term, which is positive for all ring sizes, zero is the smallest possible value for μ_2. Rings deviating more strongly from the six-membered ideal make a greater contribution to the variance. The third central moment μ_3 characterizes the skewness of a distribution. The $(n-6)^3$ term leads to negative contributions for small rings and positive contributions for large rings.

Table 1: Second and third central moment of the ring size probability distribution. The second central moment μ_2 describes the variance of a population. The larger μ_2, the broader the distribution around the mean value. The third central moment μ_3 characterizes the skewness of a population. μ_3 can take positive or negative values, depending on whether the ring sizes below or above six-membered are predominating.

Network	μ_2	μ_3
Crystalline SiO_2	0.00	0.00
Si(111) 7×7 Reconstruction	1.73	5.47
Amorphous SiO_2	1.06	0.67
Triangle Raft [17]	1.08	0.23
Graphene [18]	0.78	0.30
Cu_2O [24]	0.42	0.03
TBPB [26]	0.57	−0.09
Bubble Raft	0.57	−0.09

Crystalline SiO_2 exhibits only one ring type and, consequently, has a variance of zero and a skewness of zero. The variance of the Si 7×7 reconstruction is the largest one, since compared to the total number of rings in the unit cell, a considerable amount are deviating very much from the six-membered honeycomb. In fact, the twelve-membered ring accounts for almost half of the variance contribution. This system also is most skewed of the studied networks. The smallest variance is found for Cu_2O, where only small deviations from six-membered rings are observed. As five- and seven-membered rings are similar in number, we find the smallest skewness for Cu_2O as well (with the exception of crystalline SiO_2, of course). The variances of amorphous SiO_2 and the triangle raft [19] are very similar. The amorphous SiO_2 exhibits a larger skewness towards large rings, however. This can be explained by the fact that the upper ring size limit in Shackelford's algorithm was set to eight. Graphene [20] exhibits an average variance and skewness (compared to the other presented networks). Coincidentally, the TBPB network [28] and the bubble raft have a similar variance around the mean, and a very small skewness, due to similar contributions from small and large rings, almost cancelling out completely.

The number pair of μ_2 and μ_3 can be used to characterize the variance and skewness of a ring size distribution. Their conciseness allows very quick comparison of different networks. However, they are only attainable when detailed information is available about occurring ring sizes in the system.

The pair distance histogram (see Figure 7) expresses the probability of finding atomic positions in a certain distance from each other. The histograms that we present only cover the positions of the connection points, while ignoring the positions of other species. This can be named partial pair correlation function

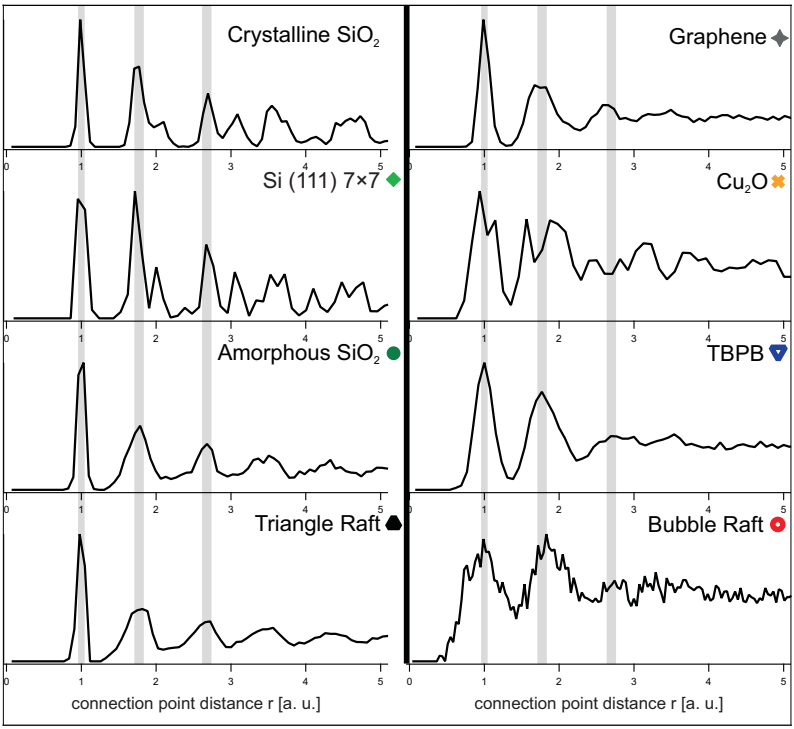

Figure 7: Pair correlation functions for connection points of all systems. All histograms have been normalized with r^{-1} to account for the number of particles in a two-dimensional gas, which increases proportional to r. Each graph has been normalized to show the first peak at 1, the original position of the first peak is given in parentheses for each system. Symbols in the upper right corner of each graph correspond to the systems' representation in Figure 6. Crystalline SiO_2 (170 connection points, first peak $0.3\,\mathrm{nm}$) and the Si 7×7 reconstruction (148 connection points, first peak $0.2\,\mathrm{nm}$) exhibit very sharp peaks that can be identified unambiguously. Amorphous SiO_2 (191 connection points, first peak $0.3\,\mathrm{nm}$) and the Shackelford triangle raft (668 connection points) appear very similar. The first three peaks are sufficiently sharp and in agreement with the peaks in crystalline SiO_2, after that, the peaks become broader. The pair correlation histogram of amorphous graphene (797 connection points, first peak $0.1\,\mathrm{nm}$) also exhibits three pronounced peaks. In the case of Cu_2O (313 connection points, first peak $0.3\,\mathrm{nm}$), the first and second peak appear split into double-peaks. The following peaks have low intensity. For the TBPB network (1994 connection points, first peak $6.5\,\mathrm{nm}$) and the bubble raft (503 connection points, first peak $2.7\,\mathrm{mm}$), only the first two peaks are clearly visible.

(PCF) or partial radial distribution function (RDF). For each possible combination of two connections points (for example two Si atoms in SiO_2), the pair distance was calculated. The resulting histogram can provide information not only on typically occurring distances in the system, but also concerning the degree of order.

A perfectly ordered crystalline system would exhibit distinct lines at lattice distances in the pair correlation function. The contrary is true for an ideal gas, which yields a continuously increasing pair correlation function without characteristic interatomic distances. Due to short range order (regular building units), amorphous materials exhibit a few maxima in the pair distance histogram, but with increasing radial distance those peaks get very broad and undefined. All histograms shown in Figure 7 were multiplied with r^{-1}. This accounts for the trivial fact that at larger distances, more positions are automatically found [34]. In the analogous three-dimensional case, a normalization factor of r^{-2} must be used instead. As we investigated structures on the atomic, the molecular and macroscopic length scales, NN distances are identified at largely differing radial distances. In order to allow straightforward comparison, all histograms were also normalized for the position of the first peak to be at 1.

In [2], partial pair distance histograms for Si-O distances, O-O distances and Si-Si distances were created from atomically resolved STM data of an amorphous SiO_2 film. By combining partial histograms into one total pair correlation function and comparing that to X-ray diffraction and neutron scattering data of bulk glass, it was verified that the first peak can be assigned to the Si-O distance within one SiO_4 tetrahedron. The next peak position describes the minimum distance for two oxygen atoms, hence characterizing the edge length of the tetrahedra. We describe only the PCF for NN distances of connection points. Hence, the first two PCF peaks, characterizing the structural building unit alone, are omitted. In the notation of A. C. Wright *et al.*, [13] the peaks of the structural building unit correspond to range I. Hence, the PCFs in Figure 7 give information on ranges II and III. Most of the systems studied in this paper exhibit a sharp first peak, indicating a narrow distribution of the connection point NN distances. In the case of crystalline SiO_2 and Si 7×7 reconstruction, all the following peaks are clearly pronounced. This behavior, demonstrating long range order, is characteristic for crystalline materials. For the amorphous SiO_2 and the triangle raft, two further peaks after the NN distance are identifiable. Their positions are in agreement with peak positions in the crystalline structure. The positions of the first three peaks in the amorphous SiO_2 film are marked in all plots with light grey bars. The amorphous graphene sheet exhibits three well-defined peaks in the PCF, the first two coincide well with the positions of amorphous SiO_2. We observe a double-peak shape for the first two peaks that occur in the PCF of Cu_2O. This feature can be assigned to the geometry of the film. The structure of $Cu_2O(111)$, which is presumed to be closely related to the film investigated by Yang *et al.*, exhibits two non-equivalent surface positions for oxygen atoms [27]. One is coordinatively saturated as an OCu_4^{2+} tetrahedron (position A), the other sits on the outmost lattice plane and is coordinatively unsaturated in OCu_3^{+} (position B). In the crystalline film, both posi-

tions alternate in the hexagonal structures and only one value (distance AB) is expected for the NN distance. It can be assumed that in the defect-rich film, coordinatively saturated und unsaturated positions are distributed randomly. When neighboring connection points happen to be the same oxygen surface position, additional bond lengths (distance AA or BB) can be the observed. However, the plane of A oxygen is geometrically equivalent to the plane of B oxygen, since they belong to the same cristobalite sublattice. It follows that the distance of AA and BB oxygen pairs is equal. The least sharp peak shapes are observed for the bubble raft connection point PCF. Since this is not a covalent network and the soap bubbles can have radii of a large range, there is no inherent limitation for the connection point NN distance. Through the experimental parameters, we have tried to produce bubbles of similar radii, so that the resulting network might be regular in A. C. Wright's range I. Apparently, this was successful, since the PCF (showing range II and III, as previously explained) exhibits two pronounced peaks and a third one with low intensity.

The PCF visualization remains an important tool when different network structures are to be compared. Starting from real space images, we are able to separate different species' positions and generate partial pair distance correlation functions. By only discussing the PCF of connection points in the network structures, we were able to investigate order in range II and III. PCFs can also be obtained *via* diffraction experiments through Fourier transformation. Discussing PCFs from real space images and from diffraction experiments helps relating two-dimensional thin film systems to their bulk analogs [2, 3].

During the introduction of the different two-dimensional network structures, we stated the observed ring sizes for each system. It is simply the next logical step, to look at characteristic clusters in which several rings are arranged. The topological cluster distribution is one of the characteristic parameters that A. C. Wright named for range III in network structures.

The Stone–Wales-like cluster is a well-known defect in the study of graphene sheets [35]. It consists of two edge-sharing seven-membered rings and five-membered rings touching on either corner of the shared edge. For brevity, it can be called a 5-7-7-5 defect. The 5-7-7-5 defect was observed in all of the unordered systems (crystalline SiO_2 and Si 7 ×7 do not exhibit the necessary ring sizes). We also examined the appearance of the structurally inverse ring combination, i.e. two edge-sharing five-membered rings and seven-membered rings touching at the corners of the shared edge or a 7-5-5-7 defect. In Figure 8, an exemplary cutout of the topography image is given for either ring cluster in all of the systems. On each cutout, a percentage value gives the occurrence probability of the defect type. The probability is determined by calculating the share that these ring clusters have in the total amount of rings. The ratios of 5-7-7-5 to 7-5-5-7 defects vary among the

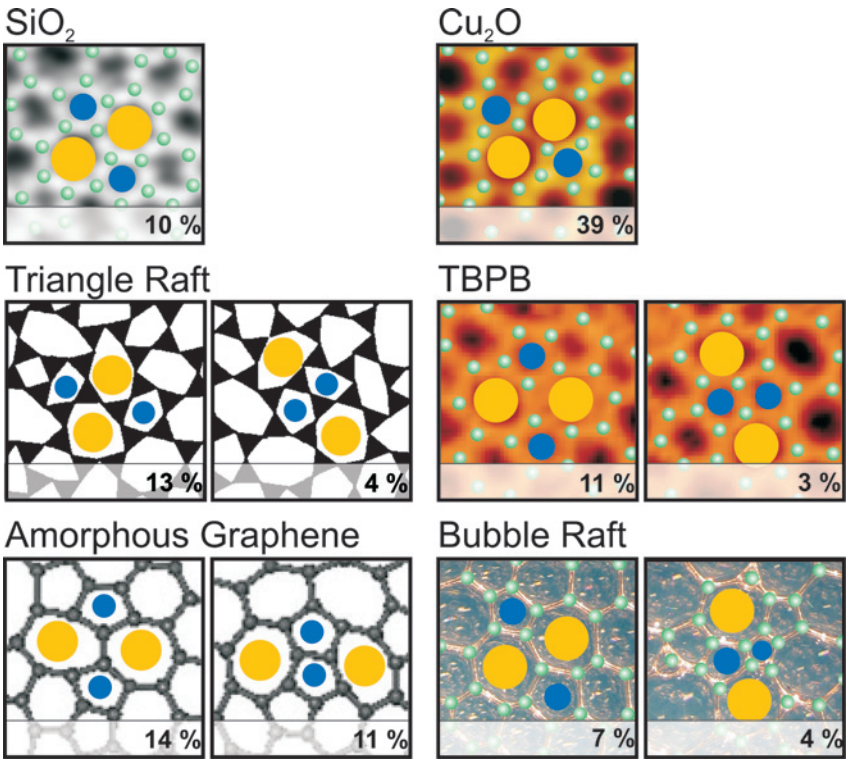

Figure 8: Density of a Stone–Wales-defect-like ring arrangement and its geometrical counterpart. The ring arrangement of two neighboring seven-membered rings and a five-membered ring on either side was observed in amorphous SiO_2, the triangle raft, amorphous graphene, Cu_2O, the TBPB network and the bubble raft. The inverse structure of two neighboring five-membered rings and a seven-membered ring in both sides occurs with a significantly lower probability in all systems. In the datasets of SiO_2 and Cu_2O that were available for this study, the inverse cluster of the Stone–Wales-arrangement was not observed. However, in other images of the amorphous SiO_2 bilayer, this cluster is found (cf. [36] supplement).

different networks, but in all investigated systems, the 5-7-7-5 defect is more abundant. A geometric consideration is proposed to explain this observation qualitatively. The geometric strain is not equal in both configurations. This will be explained for the case of silica. For the four bonds extending from one Si atom, one is stretching perpendicular to the film, connecting the bridging oxygen below. The three remaining bonds seen in the top view, can be treated for simplicities sake as parallel to the surface. The Si atom in question will be involved in the 5-7-7-5 defect, and thus connecting two seven-membered and one five-membered ring. We can therefore get a very rough estimate of the bond angle strain by adding the

internal angles for two ideal seven-membered rings and one five-membered ring ($2 \times 128.57^\circ + 108^\circ = 365.14^\circ$). The deviation of $\sim 5^\circ$ from ideal 360° gives us an idea for how much strain is induced when two seven-membered rings and a five-membered ring have to share one connection atom. We can do the same calculation for the 7-5-5-7 defect ($2 \times 108^\circ + 128.57^\circ = -344.57^\circ$) and find a larger absolute deviation of $\sim -15^\circ$. Of course, the initial occurrence probability of the involved ring sizes limits which ring clusters can be formed. How far the geometric strain influences the initial ring size distribution, depends on the particular system's ability to compensate or tolerate strain.

This qualitative geometric ansatz can be verified for a different ring arrangement. We observed 5-8-8-5 defects and 8-5-5-8 defects in the triangle raft as well as the amorphous SiO_2 film. The 5-8-8-5 defect has an angle-deviation of -18° from 360°, the 8-5-5-8 version only deviates by 9°. This is consistent with the observed occurrence in both the triangle raft and the SiO_2 film, given in the supplement.

Small ring clusters can be observed as larger recurring building units and their occurrence may be used to compare different networks. The occurrence probability of particular clusters can be estimated by calculating the geometric strain that three neighboring equilateral polyhedra exercise on a central atom.

4 Conclusion

In an effort to find unifying elements in different amorphous systems, we present a comparative study of eight two-dimensional network structures. Atomic resolution images or atomic models enable the direct determination of occurring ring sizes. We have investigated a lognormal plot of the ring size distributions and reviewed J. F. Shackelford's postulation that a lognormal distribution is an inherent feature for two-dimensional network structures [19]. Good agreement was found for an amorphous SiO_2 film, a computational amorphous graphene sheet and a TBPB network. In all of these systems, NN distances of connection points are determined by chemical bond length requirements. A stronger deviation was found for the bubble raft network, where NN distances varied to a larger extent, indicating that Shackelford's hypothesis holds if NN bond lengths are relatively uniform.

The second and third central moment of the ring size probability distribution were compared for all investigated systems. They describe the variance and skewness of a distribution. If atomic structure information is available, these characteristic variables can easily be computed.

High resolution imaging of random arrangements is an important tool for advancing the understanding of these structures. Nonetheless, the pair correlation

function, which has always been used to describe amorphous solids, remains an important tool for classifying and describing random networks. If we derive PCFs directly from image data, we have the additional option of assigning particular fragments to particular PCF peaks. In the partial PCF of the connection points, we find a similar behavior for the covalent random networks. A sharp peak indicates the NN distance, which can only have a narrow distribution for covalent networks. The bubble raft does not have inherent limitations for the NN length, and thus exhibits a broader first peak. All amorphous systems show a few further peaks that broaden progressively in range III. For a comparison, we show the PCFs of crystalline SiO_2 and a Si 7×7 reconstruction, which show well defined, periodic peaks at larger radial distances.

While the PCFs demonstrate quantitative similarities of the amorphous networks in ranges II and III, real space images complement this view in a convenient manner. Progressing from single ring size analyses, characteristic clusters of several rings can be identified and their occurrence probability in each system can be determined. The structure analogon to the Stone–Wales-defect is found in all amorphous systems. Different quartets of rings were investigated and their occurrence frequency can be qualitatively correlated with the expected bond angle strain that the involved atoms experience.

Newly available atomically resolved imaging of amorphous materials has shed new light on the nature of glass and will contribute to the development of a more detailed model of amorphous solids. It complements diffraction techniques and provides direct information on occurring structural units.

By comparing different two-dimensional network structures, common features have been identified and ways described to compare unordered networks. Taking into account that the presented amorphous silica network consists of two structurally identical layers connected by oxygen bridges, it may also be viewed as a three-dimensional model system which is extremely uniform in one direction. Hence, two four-membered rings, lying on top of each other, form a cube-shaped cage, and all larger ring-pairs form prism-shaped cages, accordingly. In naturally occurring amorphous bulk materials, this regularity cannot be expected, since no substrate registry limits the growth. The additional degree of freedom instead allows for more diverse structures. Still, cages may in principle be defined as loops that enclose a volume without any other bonds intersecting that space. Cages might then be categorized by the number of the connection points involved, or the volume enclosed. Obviously, the number of different species is expected to be higher and hence, a histogram might be less straight-forward to interpret. Further structural studies and debates will, surely, yield a more comprehensive framework for characterizing these systems.

Acknowledgement: We are grateful to Mike Thorpe and Johannes Blaschke for fruitful discussions and helpful insights.

Received August 8, 2013; accepted January 9, 2014.

References

1. W. H. Zachariasen, J. Am. Chem. Soc. **54** (1932) 3841.
2. L. Lichtenstein, C. Büchner, B. Yang, S. Shaikhutdinov, M. Heyde, M. Sierka, R. Włodarczyk, J. Sauer, and H.-J. Freund, Angew. Chem. Int. Edit. **51** (2012) 404.
3. P. Y. Huang, S. Kurasch, A. Srivastava, V. Skakalova, J. Kotakoski, A. V. Krasheninnikov, R. Hovden, Q. Mao, J. C. Meyer, J. Smet, D. A. Muller, and U. Kaiser, Nano Lett. **12** (2012) 1081.
4. R. Wiesendanger, M. Ringger, L. Rosenthaler, H. R. Hidber, P. Oelhafen, H. Rudin, and H.-J. Güntherodt, Surf. Sci. **181** (1987) 46.
5. W. Raberg and K. Wandelt, Appl. Phys. A-Mater. **66** (1998) 1143.
6. D. E. Bürgler, C. M. Schmidt, D. M. Schaller, F. Meisinger, T. M. Schaub, A. Baratoff, and H.-J. Güntherodt, Phys. Rev. B **59** (1999) 895.
7. H. Schlenz, A. Kirfel, K. Schulmeister, N. Wartner, W. Mader, W. Raberg, K. Wandelt, C. Oligschleger, S. Bender, R. Franke, J. Hormes, W. Hoffbauer, V. Lansmann, M. Jansen, N. Zotov, C. Marian, H. Putz, and J. Neuefeind, J. Non-Cryst. Solids **297** (2002) 37.
8. J.-F. Poggemann, G. Heide, and G. H. Frischat, J. Non-Cryst. Solids **326–327** (2003) 15.
9. G. H. Frischat, J.-F. Poggemann, and G. Heide, J. Non-Cryst. Solids **345–346** (2004) 197.
10. W. Raberg, A. H. Ostadrahimi, T. Kayser, and K. Wandelt, J. Non-Cryst. Solids **351** (2005) 1089.
11. G. Ertl, H. Knözinger, F. Schüth, and J. Weitkamp, *Handbook of Heterogeneous Catalysis*, Wiley-VCH, Weinheim (2008).
12. D. Weaire and N. Rivier, Contemp. Phys. **25** (1984) 59.
13. A. C. Wright, A. G. Clare, and D. I. Grimley, J. Non-Cryst. Solids **112** (1989) 33.
14. D. Löffler, J. J. Uhlrich, M. Baron, B. Yang, X. Yu, L. Lichtenstein, L. Heinke, C. Büchner, M. Heyde, S. Shaikhutdinov, H.-J. Freund, R. Włodarczyk, M. Sierka, and J. Sauer, Phys. Rev. Lett. **105** (2010) 146104.
15. R. E. Schlier and H. E. Farnsworth, J. Chem. Phys. **30** (1959) 917.
16. G. Binnig, H. Rohrer, C. Gerber, and E. Weibel, Phys. Rev. Lett. **50** (1983) 120.
17. K. Takayanagi, Y. Tanishiro, M. Takahashi, and S. Takahashi, J. Vac. Sci. Technol. A **3** (1985) 1502.
18. L. Lichtenstein, M. Heyde, and H.-J. Freund, J. Phys. Chem. C **116** (2012) 20426.
19. J. F. Shackelford and B. D. Brown, J. Non-Cryst. Solids **44** (1981) 379.
20. Y. Li and D. A. Drabold, Phys. Status Solidi B **250** (2013) 1012.
21. A. Kumar, M. Wilson, and M. F. Thorpe, J. Phys.-Condens. Mat. **24** (2012) 485003.
22. J. Kotakoski, A. V. Krasheninnikov, U. Kaiser, and J. C. Meyer, Phys. Rev. Lett. **106** (2011) 105505.
23. F. Banhart, J. Kotakoski, and A. V Krasheninnikov, ACS Nano **5** (2011) 26.
24. J. Kotakoski, J. C. Meyer, S. Kurasch, D. Santos-Cottin, U. Kaiser, and A. V. Krasheninnikov, Phys. Rev. B **83** (2011) 245420.

25. C. Gómez-Navarro, J. C. Meyer, R. S. Sundaram, A. Chuvilin, S. Kurasch, M. Burghard, K. Kern, and U. Kaiser, Nano Lett. **10** (2010) 1144.
26. F. Yang, Y. Choi, P. Liu, D. Stacchiola, J. Hrbek, and J. A. Rodriguez, J. Am. Chem. Soc. **133** (2011) 11474.
27. A. Önsten, M. Göthelid, and U. O. Karlsson, Surf. Sci. **603** (2009) 257.
28. M. O. Blunt, J. C. Russell, N. R. Champness, and P. H. Beton, Chem. Commun. **46** (2010) 7157.
29. L. Grill, M. Dyer, L. Lafferentz, M. Persson, M. V. Peters, and S. Hecht, Nat. Nanotechnol. **2** (2007) 687.
30. R. Gutzler, H. Walch, G. Eder, S. Kloft, W. M. Heckl, and M. Lackinger, Chem. Commun. **29** (2009) 4456.
31. L. Bragg and J. F. Nye, P. Roy. Soc. Lond. A Mat. **190** (1947) 474.
32. E. Limpert, W. A. Stahel, and M. Abbt, Bioscience **51** (2001) 341.
33. M. Wilson, A. Kumar, D. Sherrington, and M. F. Thorpe, Phys. Rev. B **87** (2013) 214108.
34. D. Chandler, *Introduction to Modern Statistical Mechanics*, Oxford University Press, New York (1987).
35. A. J. Stone and D. J. Wales, Chem. Phys. Lett. **128** (1986) 501.
36. L. Lichtenstein, M. Heyde, and H.-J. Freund, Phys. Rev. Lett. **109** (2012) 106101.